Current Research in Neurobiology 4 (2023) 100096

Contents lists available at ScienceDirect

Current Research in Neurobiology

journal homepage: www.sciencedirect.com/journal/current-research-in-neurobiology

Stimulus contrast modulates burst activity in the lateral geniculate nucleus

Alyssa N. Sanchez [a,1], Henry J. Alitto [a,1], Daniel L. Rathbun [b], Tucker G. Fisher [c], W. Martin Usrey [a,*]

[a] Center for Neuroscience, University of California Davis, 95618, USA
[b] Dept. of Ophthalmology, Detroit Inst. of Ophthalmology, Henry Ford Health System, Detroit, MI, 48202, USA
[c] Department of Neurobiology, Stanford University, CA, 94305, USA

ARTICLE INFO

Keywords:
Thalamus
LGN
Cat
Retina
Cortex
Coding

ABSTRACT

Burst activity is a ubiquitous feature of thalamic neurons and is well documented for visual neurons in the lateral geniculate nucleus (LGN). Although bursts are often associated with states of drowsiness, they are also known to convey visual information to cortex and are particularly effective in evoking cortical responses. The occurrence of thalamic bursts depends on (1) the inactivation gate of T-type Ca^{2+} channels (T-channels), which become de-inactivated following periods of increased membrane hyperpolarization, and (2) the opening of the T-channel activation gate, which has voltage-threshold and rate-of-change ($\delta v/\delta t$) requirements. Given the time/voltage relationship for the generation of Ca^{2+} potentials that underlie burst events, it is reasonable to predict that geniculate bursts are influenced by the luminance contrast of drifting grating stimuli, with the null phase of higher contrast stimuli evoking greater hyperpolarization followed by a larger dv/dt than the null phase of lower contrast stimuli. To determine the relationship between stimulus contrast and burst activity, we recorded the spiking activity of cat LGN neurons while presenting drifting sine-wave gratings that varied in luminance contrast. Results show that burst rate, reliability, and timing precision are significantly greater with higher contrast stimuli compared with lower contrast stimuli. Additional analysis from simultaneous recordings of synaptically connected retinal ganglion cells and LGN neurons further reveals the time/voltage dynamics underlying burst activity. Together, these results support the hypothesis that stimulus contrast and the biophysical properties underlying the state of T-type Ca^{2+} channels interact to influence burst activity, presumably to facilitate thalamocortical communication and stimulus detection.

1. Introduction

Visual information reaches the cerebral cortex primarily via the retino-geniculo-cortical pathway. Neurons in the lateral geniculate nucleus (LGN) of the thalamus receive direct input from retinal ganglion cells and convey this information to target neurons in primary visual cortex (V1). Although LGN projection neurons are often viewed as passive relay cells, they are known to transform retinal signals in several dynamic ways, including transformations in the temporal domain (Dan et al., 1996; Usrey et al., 1998; Wang et al., 2007; Martinez et al., 2014; Butts et al., 2016; Fisher et al., 2017; Alitto et al., 2019b). A prominent example of such a transformation is the shift in LGN firing between tonic spiking and burst spiking (reviewed in Sherman and Guillery, 2009; Usrey and Alitto, 2015; Usrey and Sherman, 2022). Importantly, LGN neurons switch between these two forms of spiking based on the time/voltage history of their membrane potential (Jahnsen and Llinás, 1984). Thus, these two types of activity, tonic activity and burst activity, could be differentially engaged by distinct patterns of visual stimulation and, consequently, be used to differentially encode information about stimuli being provided to cortex. This view is supported by past work showing bursts can transmit visual information and occur reliably to specific patterns of visual stimuli (Guido et al., 1995; Reinagel et al., 1999; Rivadulla et al., 2003; Lesica and Stanley, 2004; Alitto et al., 2005).

LGN projection neurons in tonic mode respond to excitatory inputs with regularly spaced action potentials, generally in proportion to the strength of the stimulus (Llinás and Jahnsen, 1982; Huguenard and McCormick, 1992). In comparison, LGN projection neurons in burst mode generate tight clusters of spikes, referred to as "bursts". Whether or not LGN neurons produce tonic or burst spikes depends on the state of

* Corresponding author. Center for Neuroscience, University of California, 1544 Newton Court, Davis, CA 95618, USA.
E-mail address: wmusrey@ucdavis.edu (W.M. Usrey).
[1] Contributed equally to this study.

https://doi.org/10.1016/j.crneur.2023.100096
Received 7 December 2022; Received in revised form 3 June 2023; Accepted 8 June 2023
Available online 10 June 2023
2665-945X/© 2023 The Authors. Published by Elsevier B.V. This is an open access article under the CC BY-NC-ND license (http://creativecommons.org/licenses/by-nc-nd/4.0/).

their voltage-gated, T-type Ca^{2+} channels (or T-channels). T-channels have two gates, an inactivation gate and an activation gate (Tsien et al., 1988; Crunelli et al., 2005). Once T-channels are de-inactivated following a sufficient period of hyperpolarization, an appropriate depolarizing stimulus can open the activation gate, thereby generating a depolarizing Ca^{2+} potential (or T-potential; McCormick and Huguenard, 1992 Huguenard and McCormick, 1992; Huguenard, 1996; Perez-Reyes, 2003). If the T-potential crosses the threshold to open voltage-gated Na^{+} channels, then a short train of high-frequency, Na^{+}-based action potentials, referred to as a burst, will result (Suzuki and Rogawski, 1989; McCormick and Huguenard, 1992; Huguenard and McCormick, 1992; Huguenard, 1996; Perez-Reyes, 2003). Notably, the magnitude of the T-potential and the number of spikes in a burst depend on (1) the ratio of T-channels in the de-inactivated vs. inactivated state, which depends, in turn, on the depth and duration of hyperpolarization in the cell, and (2) the subsequent rate of depolarizing voltage change ($\delta v/\delta t$) (Deschênes et al., 1984; Destexhe and Sejnowski, 2002; Hong et al., 2014). If the T-channels are primarily in the inactivated state or the depolarization is too slow, then tonic spiking occurs. Although visually evoked bursts are more common in anesthetized and drowsy animals than in alert animals, visually evoked bursts occur across brain states (Weyand et al., 2001; Bezdudnaya et al., 2006; Bereshpolova et al., 2011) and, when they occur, burst spikes are particularly effective in evoking cortical responses (Swadlow and Gusev, 2001; see also Usrey et al., 1998) and increase the timing precision and spatial focus of cortical responses (Borden et al., 2022).

Across mammals, the majority of LGN neurons have either On-center or Off-center receptive fields (Kuffler, 1953; Hubel and Wiesel, 1961), the former being (i) depolarized by light increments over the center of their receptive fields and (ii) hyperpolarized by light decrements over the same region, and the latter showing the reverse pattern. With these receptive-field properties in mind, a drifting grating stimulus should evoke alternating periods of depolarization and hyperpolarization in both types of cells, with the magnitude of hyperpolarization and depolarization and the rate of voltage change, being dictated by the contrast and phase of the time varying stimulus (Wang et al., 2007). Based on these properties and assumptions, we made single-unit recordings from LGN neurons in the anesthetized cat to test the hypothesis that bursts are affected by stimulus contrast, with burst activity being more frequent and temporally precise with higher contrast stimuli compared with lower contrast stimuli. We also performed simultaneous intraocular and LGN recordings to examine the spiking patterns of synaptically connected retinal ganglion cells and LGN neurons to compare the influence of contrast on the relationship between interspike interval and retinogeniculate communication and high-frequency responses in the LGN. Results show that bursts occur more frequently with higher contrast stimuli and more consistently with respect to the phase of the stimulus cycle when compared to tonic spikes. These results support the view that burst and tonic firing modes can differentially encode information about visual stimuli and the external world.

2. Materials and methods

2.1. Animal preparation

Ten adult cats, both sexes, were used for this study. All experimental procedures were conducted with the consent of the Animal Care and Use Committee at the University of California, Davis and followed National Institutes of Health guidelines. The analyses performed on spikes trains for this study come from a combination of new unpublished data and data that contributed to previous, but unrelated, studies on the retinogeniculate pathway (Alitto et al., 2019b; Rathbun et al., 2010, 2016).

All surgical procedures were performed while animals were anesthetized. Surgical anesthesia was induced with ketamine (10 mg/kg, i. m.) and xylazine/dexmedetomidine (1 mg/kg, i. m.) and maintained with either thiopental sodium (20 mg/kg, i. v., supplemented as needed) or propofol (4–6 mg/kg/h, i. v., supplemented as needed) and sufentanil citrate (0.1–25 μg/kg/h, i. v., supplemented as needed) along with isoflurane (0.5–1.5%) in a 2:1 mix of oxygen and nitrous oxide. Tracheotomies were performed, and animals were placed in a stereotaxic apparatus where they were mechanically ventilated and given atropine (0.04 mg/kg, i. m.), dexamethasone (0.2 mg/kg, i. m.), and baytril (5 mg/kg, i. m.). Animals' vitals were monitored throughout the experiment, including the EEG, ECG, CO_2, and temperature. If physiological monitoring indicated a decreased level of anesthesia (increased heart rate, CO_2, and/or high-frequency activity in the EEG), additional thiopental sodium or propofol and sufentanil citrate was given, and the rate of continuous infusion was increased. For each animal, a scalp incision was made, and skin edges were infused with lidocaine (2%). A single craniotomy was made over the LGN, the dura was removed, and the craniotomy was filled with agarose to protect the underlying brain. Eyes were fixed and adhered to metal posts, fitted with contact lenses, and focused on a tangent screen located 172 cm in front of the animal. Flurbiprofen sodium drops were administered (0.3%) to prevent miosis, atropine drops were administered (1%) for pupil dilation, and phenylephrine drops (2.5%) were administered to retract the nictitating membranes. Once all surgical procedures were complete, animals remained anesthetized with maintenance doses of anesthetic agents (either thiopental sodium, 2–3 mg/kg/h, i. v. Or propofol, 4–6 mg/kg/h, i. v., and sufentanil citrate, 0.1–25 μg/kg/h, i. v., and isoflurane, 0.1–0.5% in a 2:1 mix of oxygen and nitrous oxide). Before administering paralytic, animals were monitored for 1 h to ensure a stable plane of anesthesia. Once a steady plane of maintenance anesthesia was established, animals were paralyzed with vecuronium bromide (0.2 mg/kg/h, i. v.). At the end of data collection, animals were euthanized with Euthasol (100 mg/kg, i. v.).

2.2. Electrophysiological recording and visual stimuli

Single-unit extracellular recordings were made from LGN cells in layers A and A1 using parylene-coated tungsten electrodes (AM systems, Sequim, WA). In a subset of experiments, a second electrode was inserted into the retina to provide simultaneous recordings from synaptically connected retinal ganglion cells and LGN neurons (procedures described in Alitto et al., 2019b; Rathbun et al., 2010, 2016). Neural responses were amplified, filtered, and recorded to a computer equipped with a Power 1401 data acquisition interface and Spike 2 software package (Cambridge Electronic Design, Cambridge, UK). Spike isolation was based upon waveform analysis and the presence of a refractory period, assessed from the autocorrelogram.

Visual stimuli were generated using a VSG2/5 visual stimulus generator (Cambridge Research Systems, Rochester, UK) and presented on a gamma-calibrated Sony monitor running at 140 Hz. Mean luminance of the monitor was 38 cd/m^2. The visual responses of individual LGN neurons were mapped and assessed using white-noise stimuli and drifting sine-wave gratings. White-noise stimuli consisted of a 16 by 16 grid of black and white squares. Each square was temporally modulated according to a 2^{15}-1 length m-sequence (Sutter, 1987; Reinagel et al., 1999; Reinagel et al., 1999). Individual squares in the stimulus were updated with each monitor frame (~4 min for a complete sequence). Between 4 and 16 squares of the stimulus overlapped receptive field centers of each individual neuron. White-noise stimuli were used to quantify the spatiotemporal receptive field properties of each cell for purposes of cell classification (Usrey et al., 1999). We also determined each cell's preferred size and spatial frequency using drifting sine-wave gratings (4 Hz) centered over the cell's receptive field. Once the preferred location, size, and spatial frequency were determined, cells were presented with multiple repeats of a drifting grating stimulus that varied in contrast (2.5%, 5%, 10%, 20%, 40%, 60%, 80%, and 100%; random order). With each repeat of the stimulus, gratings were shown for 4 s and were interleaved with 4 s of mean gray.

2.3. Identification of LGN burst and tonic spikes

We used two well-established criteria to identify bursts in the spike trains of LGN neurons, (Lu et al., 1992; Swadlow and Gusev, 2001; Weyand et al., 2001; Lesica and Stanley, 2004; Alitto et al., 2005, 2011, 2019b; Denning and Reinagel, 2005; Bezdudnaya et al., 2006; Bereshpolova et al., 2011). These criteria were: (1) a preceding interspike interval (ISI) of >100 ms, and (2) one or more subsequent spikes that followed with ISIs of <4 ms (Fig. 1). Spikes that met these criteria were labeled burst spikes, and all other spikes were labeled tonic spikes. The first spike of a burst is referred to as the cardinal spike. Some of the analyses used the cardinal spike of each burst to represent a burst "event", whereas others used all spikes within a burst (described below). Throughout the paper, we use the terms long-ISI and high-frequency events to refer to the first and second criteria for a burst, respectively.

2.4. Tonic vs. burst analysis: firing rate

Burst and tonic responses that occurred during low- and high-contrast stimulation were compared. The cutoff for low- and high-contrast stimuli was based each cell's contrast response function, where the low-contrast condition was any contrast value that elicited ≤30% of maximum firing rate and the high-contrast condition was any contrast value that elicited ≥75% of maximum firing rate of the cell. For the high- and low-contrast conditions, we calculated the firing rate of burst and tonic spikes as well as the average number of spikes within each burst event. To quantify the contrast-dependent changes in tonic and burst activity, we calculated a modulation index at each contrast level. The modulation index for each cell was calculated as follows:

$$modulation\ index(x) = \frac{firing\ rate(x) - firing\ rate_{spontaneous}}{firing\ rate(x) + firing\ rate_{spontaneous}}$$

Here, x = stimulus contrast. Tonic f1 was used for tonic firing rate, while bursts/cycle was used for the burst firing rate (i.e., bursts per cycle of the drifting grating). To compare the modulation indices across cells, we computed the effective contrast:

$$effective\ contrast\ (x) = \frac{firing\ rate(x)}{\max\ (firing\ rate)}$$

For example, if the cell's response was 20 spikes/s at 30% contrast, with a maximum firing rate of 40 spikes/s, then the effective contrast was 0.5.

2.5. Tonic vs. burst analysis: pairwise phase consistency

To assess response timing across the stimulus cycle, we calculated Pairwise Phase Consistency (PPC) for tonic and burst spikes across different contrast conditions (Vinck et al., 2010). The phase for each spike (burst or tonic, spike time relative to stimulus onset) at the drift rate of the visual stimulus (4 Hz) was calculated as:

$$\Phi_i = 2\pi * \frac{modulus(spike\ time_i, cycle\ duration)}{cycle\ duration}$$

PPC was then calculated for each spiking category (burst vs tonic) and each stimulus condition (low vs high contrast):

$$ppc = \sum_i \sum_{j<i} \frac{\cos\ \Phi_i * \cos\ \Phi_j + \sin\ \Phi_i * \sin\ \Phi_j}{.5n(n-1)}$$

Here, n is the number of spikes in each category/condition. Low PPC values near zero indicate no consistent relationship between the spike timing and phase of the visual stimulus, whereas PPC values near 1.0 indicate that the spikes always occur at the same phase of the visual stimulus.

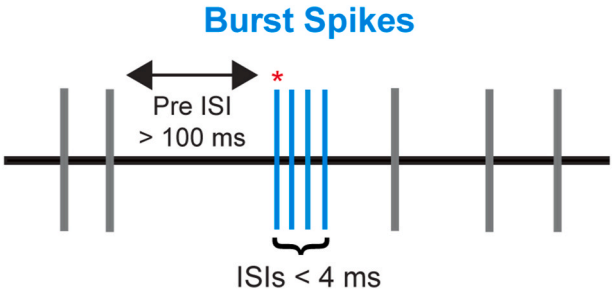

Fig. 1. Identification of burst spikes using criteria established by Lu et al. (1992). In this diagram, time is moving left to right and the vertical lines indicate spikes. Bursts are defined as (i) a cardinal spike (indicated with red *) that follows an ISI >100 ms, and (ii) subsequent spikes that occur with ISIs <4 ms. In this example, the burst spikes are shown in blue and the tonic spikes are shown in gray. (For interpretation of the references to colour in this figure legend, the reader is referred to the Web version of this article.)

2.6. Retinal spike efficacy

To quantify the influence of contrast-dependent bursting on retinogeniculate communication, we measured the retinal efficacy (percentage of retinal spikes that evoked a postsynaptic spike or burst event) for a subpopulation of the LGN cells (n = 14) in which simultaneous recordings were made from one of their retinal inputs (via intraocular recordings) as a function of ongoing LGN ISI during high- and low-contrast conditions. Synaptic connectivity was assessed using cross-correlation analysis, as described in Fisher et al. (2017). Changes in retinal spike efficacy were assessed as a function of ongoing LGN ISI, which is defined as the time since the previous LGN spike at the time of a given retinal spike. For example, if a retinal spike occurred at 3.753 s and the last LGN spike occurred at 3.750s, then the retinal spike is said to occur during a 0.003 ongoing LGN ISI. We have previously shown that ongoing LGN ISI can be used as a reliable proxy for burst probability (Alitto et al., 2019b). In particular, (1) the probability of a high-frequency LGN event increases as the LGN ISI increases beyond 50 ms, in a manner that cannot be explained by passive mechanisms, indicating the likely involvement of T-Type Ca^{2+} channels, and (2) coincident with the increase of high-frequency probability at long LGN ISIs, there is an increase in retinal spike efficacy that is also difficult to explain by passive mechanisms. To quantify the relationship between contrast-dependent changes in retinal spike efficacy and contrast-dependent changes in LGN burst rate at long LGN ISIs, we modeled changes in retinal spike efficacy using generalized linear mixed-effects model (fitglme, Matlab version R2021a, MathWorks) with predictors of tonic f1, burst rate, and stimulus contrast. Cell identity was used as a random variable.

2.7. Poisson expectation of thalamic burst rate

To address the possibility that changes in contrast-dependent burst rates were simply a statistical consequence of overall changes in firing rate, we estimated the frequency of burst events from a nonhomogeneous Poisson spiking model. Spike times were simulated based on a time-varying sinusoidal function where firing rates were set by the cell's f1 and f0:

mean spike count (t) = f1*sin(2*pi*t*f) + f0

Here, t = time, f = the drift frequency of the visual stimulus, f1 = response at the frequency of the visual stimulus, and f0 = mean response. The sinusoidal model was then rectified such that negative spike counts were set to zero. For each LGN neuron, 100 trials were simulated: 4s stimulus on, 4s stimulus off, to match how the experimental data was collected. Simulated spike trains were analyzed similar to the experimental data to quantify the amount of burst activity that would be predicted to occur simply as a result of the cell's firing rate. For

each neuron, the mean and standard deviation of the simulated data were estimated through bootstrap to determine if the neuron's experimental burst rate was significantly greater than that found in the simulated data.

2.8. Statistical testing

All analyses were done in Matlab version 2021a. For significance testing, t-tests were used for normally distributed variables (verified with a Kolmogorov–Smirnov test); sign tests were used for non-normally distributed variables (e.g., bounded indices).

3. Results

We recorded a total of 511,002 spikes (including 39,107 burst events comprised of 90,068 burst spikes) from 21 LGN neurons (11 on-center cells, 10 off-center cells; 6 X cells, 15 Y cells) in the anesthetized cat during visual stimulation with drifting sinusoidal gratings that varied in luminance contrast to determine the relationship between stimulus contrast and burst versus tonic spiking. For the analyses described below, there were not any statistically significant differences between subtypes of LGN cells (on vs. off, X vs. Y). For a subset of the LGN cells (n = 14; 373,325 spikes, total) we also simultaneously recorded the spiking activity of one of their retinal ganglion cell inputs (999,044 retinal spikes, total) via a second electrode inserted into the eye. We were particularly interested in determining whether high-contrast stimuli, with presumably greater null phase hyperpolarization for priming T-type Ca^{2+} channels and a greater rate of depolarization ($\delta v/\delta t$) during the transition from the null phase to the preferred phase, evoked more geniculate bursts than low-contrast stimuli. Recordings were divided into low- and high-contrast trials based on each cell's contrast response function (see Materials and Methods). Geniculate spikes were classified as burst or tonic using previously established criteria (Lu et al., 1992), whereby a burst has a sequence of two or more spikes, with the initial spike having a preceding interspike interval (ISI) > 100 ms and subsequent spikes having ISIs < 4ms (Fig. 1). All non-burst spikes were classified as tonic spikes.

3.1. Thalamic bursting is modulated by stimulus contrast

On average, bursting events were more common (>2x more frequent) with high-contrast stimuli than they were with low-contrast stimuli. This contrast-dependent increase in LGN bursting was clearly observed in single-cell raster plots (Fig. 2A and B), PSTHs (Fig. 2C and

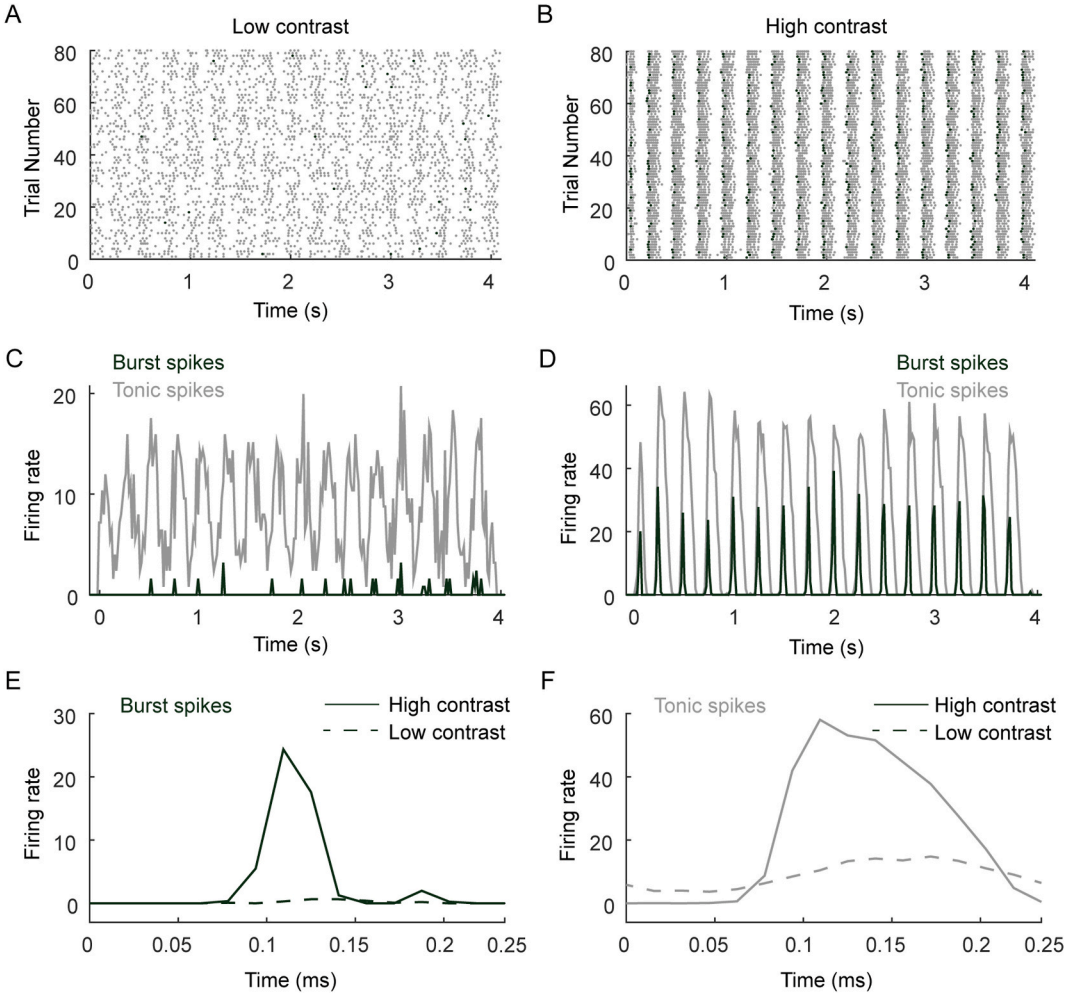

Fig. 2. Burst and tonic responses from a representative LGN neuron during high- and low-contrast visual stimulation. **A** and **B**. Raster plots showing the neuron's spiking activity across 80 4-s trials of a 4 Hz drifting sinusoidal grating stimulus at low contrast (**A**) and high contrast (**B**; see Materials and Methods). Burst spikes indicated in dark green; tonic spikes indicated in shades of gray. Note: at the time scale shown, the multiple spikes that occur during a single burst appear as a single marker. **C** and **D**. PSTHs showing the firing rate of burst spikes (dark green) and tonic spikes (shades of gray) during stimulation with (**C**) low-contrast drifting gratings and (**D**) high-contrast drifting gratings. **E** and **F**. Cycle histograms showing the relative timing and duration of burst spikes (**E**) and tonic spikes (**F**) with low-contrast drifting gratings (dashed lines) and high-contrast drifting gratings (solid lines).

D), and cycle histograms (Fig. 2E and F) and was robust across our sample of LGN neurons (Fig. 3A; mean burst events per cycle: high contrast = 0.27 ± 0.01, low contrast = 0.12 ± 0.01, $p < 10^{-3}$, *t*-test). There was also a small, but significant, increase in the number of spikes within a burst with high-contrast stimuli compared to low-contrast stimuli (Fig. 3B; mean spikes/burst: high contrast = 2.25 ± 0.03, low contrast = 2.15 ± 0.03; p = 0.03, *t*-test). Across cells, the contrast response function for burst spikes was similar in shape to the contrast response function for tonic spikes (Fig. 3C); however, the influence of contrast on bursting activity was weaker than the influence of contrast on tonic spikes, particularly at high contrasts where tonic spikes have a higher ceiling (limited by the action potential refractory periods) than burst spikes (limited by the 100 ms ISI lockout period). This can be seen by plotting the contrast modulation index as a function of effective contrast (see Materials and Methods) for both tonic and burst spikes across the sample of LGN neurons (Fig. 3C). Comparing the modulation index for burst spikes and tonic spikes, the modulation index covaries for both burst and tonic firing, and it is higher for tonic spikes compared to bursts. This reflects the upper bound on the two categories of spikes; bursts can only happen once per cycle (due to the 100ms lockout), whereas tonic spikes can occur more than once. Overall, there was a tight correlation between the modulation of tonic spiking and burst spiking across all contrasts (Fig. 3D, r = 0.7, $p < 10^{-4}$).

Having found a positive relationship between stimulus contrast and burst probability, we next asked whether stimulus contrast affected the consistency of burst activity within the temporal domain. To address this question, we performed a Pairwise Phase Consistency (PPC) analysis to quantify the consistency of the stimulus phase when bursts occurred (see Materials and Methods). With this analysis, higher PPC values indicate greater consistency of responses with respect to stimulus phase and lower values indicate less consistency. On average, PPC values for burst activity were significantly greater for high-contrast stimuli than for low-contrast stimuli (Fig. 4A; high-contrast mean PPC = 0.67 ± 0.06, low-contrast mean PPC = 0.44 ± 0.06; $p = 7.29 \times 10^{-4}$, sign test. A similar relationship was also found for tonic spikes (Fig. 4B; high contrast mean PPC = 0.47 ± 0.05, low contrast mean PPC = 0.35 ± 0.05; p = 0.002, sign test); however, across cells and contrast values, PPC values were typically greater for bursts than for tonic spikes (Fig. 4C and D; low-contrast: burst PPC vs. tonic PPC, p = 0.019, sign test; high contrast: burst PPC vs. tonic PPC, p = 0.007, sign test). Thus, high-contrast stimuli are more likely to evoke bursts than low-contrast stimuli, and bursts under high-contrast conditions have greater phase consistency. Both features are consistent with the notion that bursts can carry contrast information to the cortex.

3.2. *Changes in retinal spike efficacy can be partially explained by contrast-dependent changes in bursting*

Previous work has shown that the ability of retinal spikes to drive spiking in the LGN (retinal spike efficacy) is modulated by bursting in the LGN (Alitto et al., 2019b). Although this work did not directly measure LGN Ca^{2+} potentials, the relative arrival of retinal spikes to the

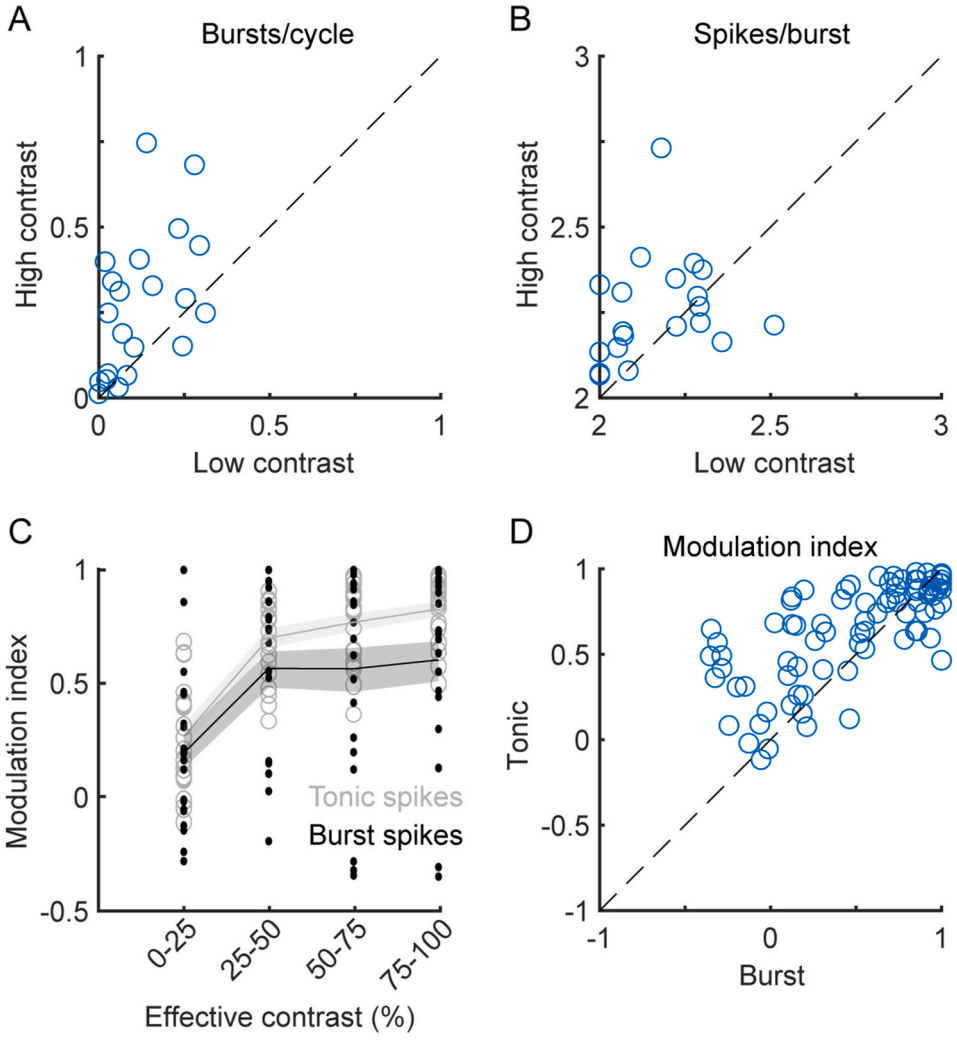

Fig. 3. Burst activity during high- and low-contrast visual stimulation. **A.** Scatter plot showing the average burst rate (burst events per cycle of the drifting grating stimulus) for 21 LGN neurons stimulated with high- and low-contrast gratings. Burst rate is significantly greater for high-contrast stimuli compared to low-contrast stimuli ($p < 10^{-3}$, *t*-test). **B.** Scatterplot showing the average number of spikes per burst for 21 neurons stimulated with high- and low-contrast gratings. There was a small, but significant, increase in the number of spikes per burst with high-contrast stimuli compared to low-contrast stimuli (p = 0.03, *t*-test). **C.** Modulation index as a function of effective contrast (see Materials and Methods). At each effective contrast level, gray circles represent the modulation index of tonic spikes for each neuron examined at that contrast, and black dots represent the modulation index of burst spikes for each neuron examined at that contrast (tonic spikes (gray circles and gray line): mean ± ste = 0.27± 0.05, 0.70± 0.04, 0.77± 0.04, 0.82± 0.03 for 25%, 50%, 75%, and 100% contrast, respectively; burst spikes (black dot and black line): mean ± ste = 0.19± 0.08, 0.56± 0.08, 0.56 ±0.10, 0.60±0.09 for 25%, 50%, 75%, and 100% contrast, respectively). **D.** Scatterplot showing the burst modulation index versus the tonic modulation index. The modulation index was significantly greater for tonic spikes than for burst spikes (tonic: mean 0.638± 0.032 ste; burst: mean 0,483± 0.047 ste, p = 0.0198 sign test).

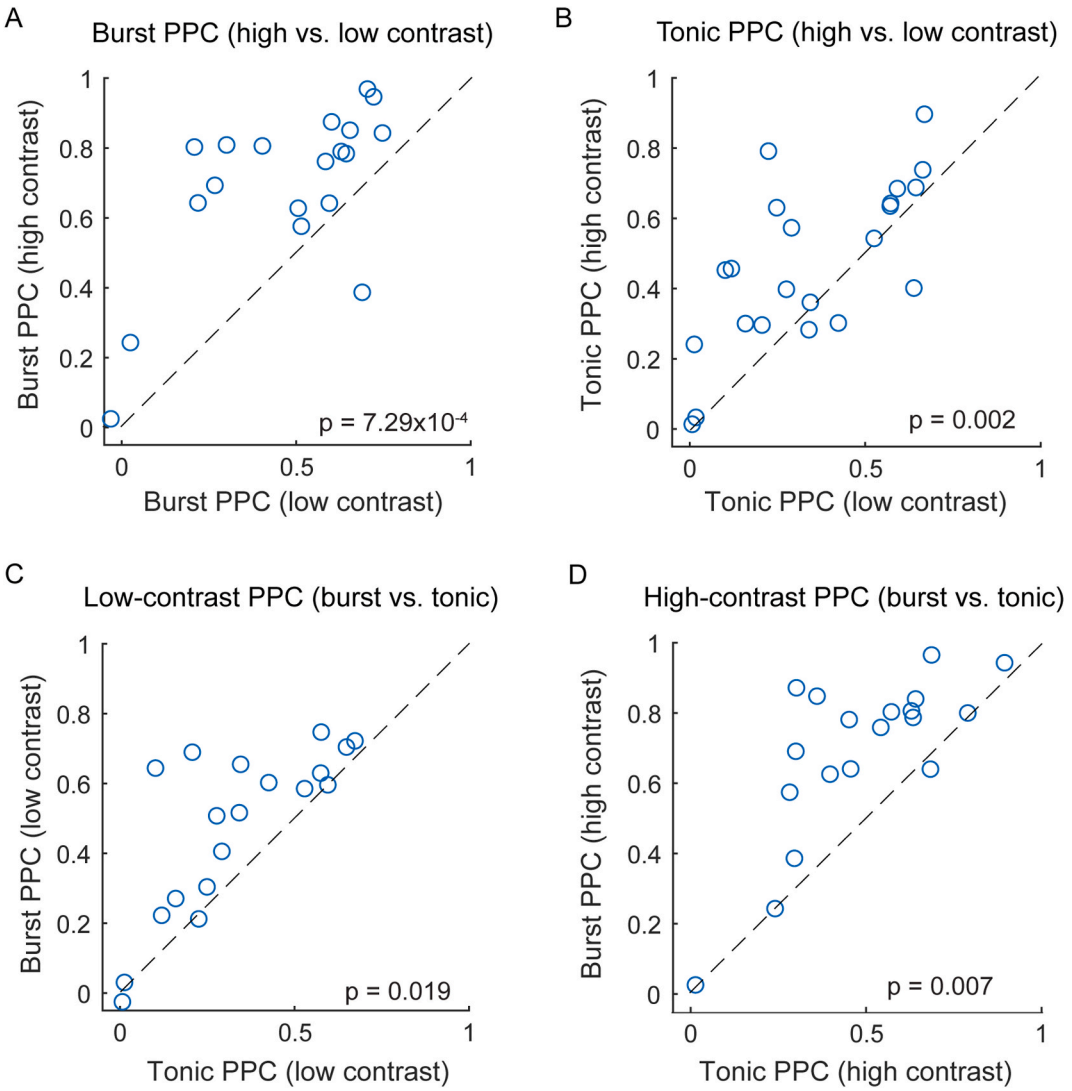

Fig. 4. Scatterplots showing pairwise phase consistency (PPC) values for burst and tonic spikes when stimulated with low- and high-contrast gratings. **A** and **B**. Comparison of PPC values from recordings with high-contrast and low-contrast stimulation for burst spikes (**A**) and tonic spikes (**B**). PPC values for burst spikes and tonic spikes were significantly greater, on average, when cells were stimulated with high-contrast stimuli compared with low-contrast stimuli ($p = 7.29 \times 10^{-4}$ and $p = 0.002$, respectively; sign test). **C** and **D**. On average, PPC values were greater for burst spikes than for tonic spikes when cells were excited with low-contrast stimuli (**C**, $p = 0.019$, sign test) and when excited with high-contrast stimuli (**D**; $p = 0.007$, sign test).

time since a previous LGN spike (ongoing LGN ISI, $ISI_{ongoing}$; see Materials and Methods) influenced several aspects of visual processing in the LGN, including retinal spike efficacy, in a manner consistent with the biophysics of T-type Ca^{2+} channels. In this way, $ISI_{ongoing}$ can be used to infer the relative probability of thalamic burst mode in a manner that is complementary to the traditional criteria.

To examine the relationship between retinal spike efficacy and burst probability under low- and high-contrast conditions, we analyzed the spike trains of synaptically connected retinal ganglion cells and LGN neurons (see Materials and Methods). Fig. 5A1, 5B1, and 5C1 show the relationship between ongoing ISI and retinal efficacy for 3 representative pairs of synaptically connected neurons. Also depicted in these figures (gray shading) are 3 ranges of ongoing ISI that were used to compare the probability of retinal evoked geniculate spikes under low- and high-contrast conditions (Fig. 5A2-A4, B2-B4, C2-C4). Results from these 3 examples and the entire sample of simultaneously recorded neurons (Fig. 5D1) show that the relationship between retinal spike efficacy and burst probability, as assessed by $ISI_{ongoing}$, is highly nonlinear. Specifically, when the $ISI_{ongoing}$ is short (<30ms; indicated with black arrow in A1-D1) and Ca^{2+} potentials are unlikely to occur, there is a negative relationship between retinal efficacy and $ISI_{ongoing}$. Interestingly, in this region of the ISI-efficacy curve, low-contrast spikes are more effective than high-contrast spikes in driving LGN activity, particularly at the shortest $ISI_{ongoing}$ (<30ms, zone 2 in panels A1, B1, and C1). This finding is consistent with LGN contrast gain control mechanisms, similar to what has been previously reported (Alitto et al., 2019a).

More importantly for the current study, our results reveal a contrast-dependent increase in retinal spike efficacy as the $ISI_{ongoing}$ increases beyond 50ms and the probability of burst mode increases. To quantify this contrast-dependent effect, we compared retinal spike efficacy found during mid-duration $ISI_{ongoing}$ (30–60ms, zone 3 in panels A1, B1, and C1) to long-duration $ISI_{ongoing}$ (>100ms, zone 4 in panels A1, B1, and C1) (Fig. 5D2). These specific ranges were selected to exclude the short-duration $ISI_{ongoing}$ range where temporal summation dominates ISI-efficacy curves. Results show a significant increase in retinal spike efficacy during long-duration $ISI_{ongoing}$ relative to mid-duration $ISI_{ongoing}$ with both high- and low-contrast stimuli (high-contrast stimuli: retinal efficacy with mid-duration $ISI_{ongoing} = 0.053 \pm 0.012$, with long-duration $ISI_{ongoing} = 0.161 \pm 0.024$, $p = 9.76 \times 10^{-4}$; low-contrast stimuli: retinal

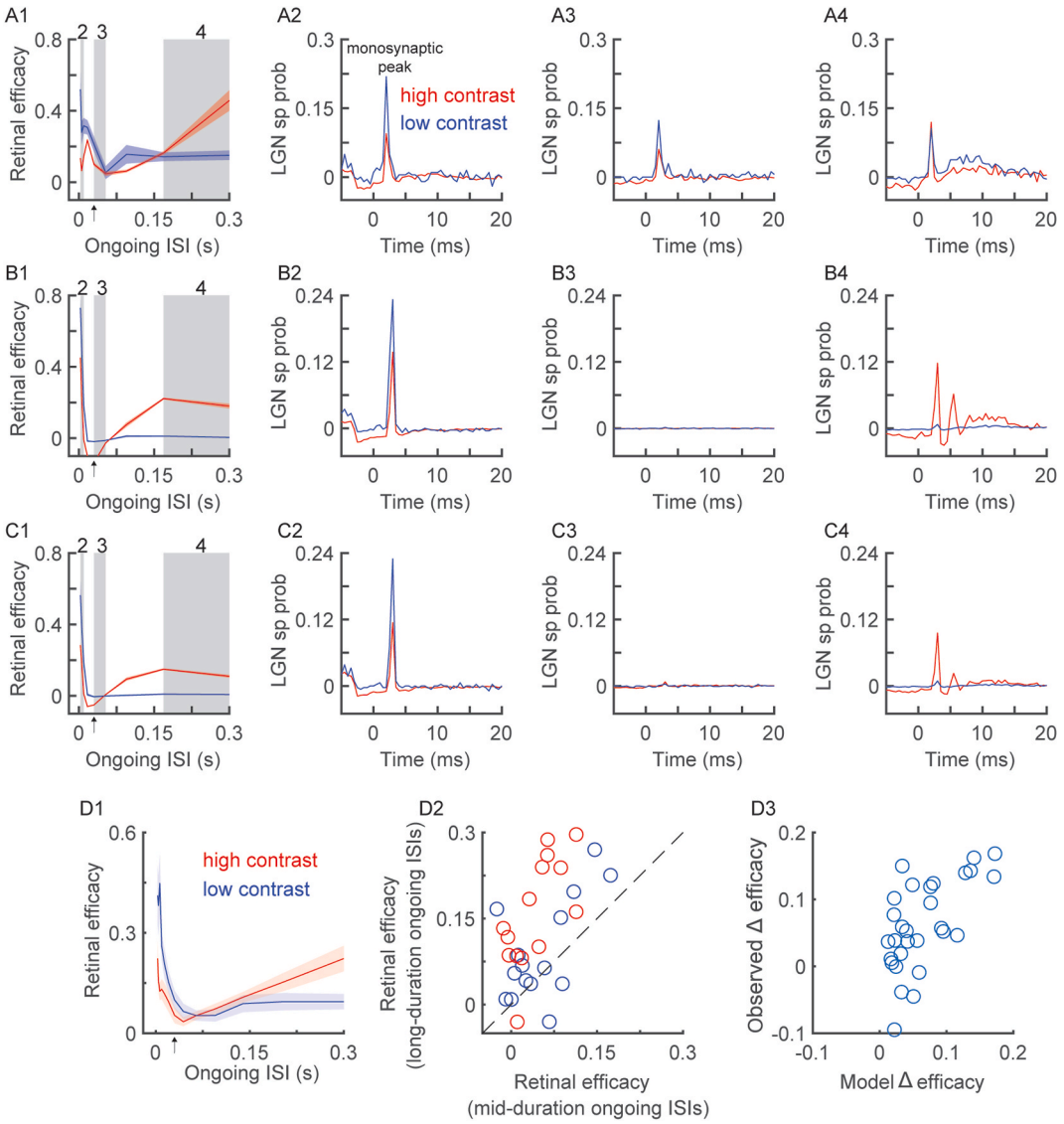

Fig. 5. The relationship between contrast-dependent retinal spike efficacy and contrast-dependent burst rate. **A1.** Example ongoing ISI-efficacy curves for low-contrast (blue) and high-contrast (red) trials. The three gray boxes indicate three regions of interest: (2) short-ongoing LGN ISIs (<30ms) where retinal spike efficacy is dominated by temporal summation, (3) mid-duration ongoing LGN ISIs (30–60ms) where retinal spike efficacy is at a minimum, and (4) long-duration ongoing LGN ISIs (>100ms) where the inferred activation of T-Type Ca^{2+} channels enhances retinal spike efficacy. The data are binned logarithmically. Arrow indicates where the ongoing ISI is 30ms. **A2.** LGN spike probability as a function of time since a retinal spike for short-ongoing ISIs, as defined above. The peak near 3.0 ms indicates a monosynaptic connection between the RGC-LGN pair. The area under the curve is used to calculate spike efficacy. **A3.** Similar to A1, but for mid-duration ongoing LGN ISIs. **A4.** Similar to A1, but for long-ongoing LGN ISIs. **B–C.** Similar to A for two additional example RGC-LGN pairs. **D1.** Similar to A1, but for the entire sample of RGC-LGN pairs. **D2.** Scatter plot of retinal efficacy during mid-duration ongoing LGN ISIs vs. retinal efficacy during long-duration ongoing LGN ISIs (low contrast: $p = 9.76 \times 10^{-4}$; high contrast: $p = 0.007$, sign test). **D3.** A scatter plot of observed change in retinal spike efficacy plotted as a function of the output of a generalized linear model with significant predictors of burst rate and spike f1 ($ß_{burst} = 0.024$, tstat = 2.24, $p = 0.01$; $ß_{f1} = 0.026$, tstat = 2.59, $p = 0.02$). (For interpretation of the references to colour in this figure legend, the reader is referred to the Web version of this article.)

efficacy with mid-duration $ISI_{ongoing} = 0.053 \pm 0.015$, with long-duration $ISI_{ongoing} = 0.092 \pm 0.023$, $p = 0.007$, sign test); however, the effect was significantly greater with high-contrast stimuli ($p = 0.007$, sign test), and may include a component involving convergent input from other, non-recorded, retinal ganglion cells.

To establish a more direct link between contrast-dependent changes in ISI-efficacy curves and burst rate, we next created a generalized linear mixed-effects model of the change in spike efficacy (Δ_{eff}) using contrast, burst rate, and the fundamental frequency (f1) of the spiking response. This simple linear model did a good job at predicting Δ_{eff} observed between mid-duration and long-duration $ISI_{ongoing}$ (Fig. 5D3, explained variance = 0.4). Both burst rate and f1 were significantly positive predictors of Δ_{eff} ($ß_{burst} = 0.024$, tstat = 2.24, $p = 0.01$; $ß_{f1} = 0.026$, tstat = 2.59, $p = 0.02$), while contrast was not predictive of Δ_{eff} ($ß_{con} = -0.007$, tstat = 0.24, $p = 0.81$). This indicates an indirect relationship between contrast and Δ_{eff}. One parsimonious explanation of these results is that changing contrast drives changes in burst rate, which is a reliable proxy for an underlying neural mechanism, (e.g., state of the T-Type Ca^{2+} channels), that then drives the Δ_{eff}. Mathematically, this indirect relationship between stimulus contrast and Δeff is supported by the finding that contrast is a significant predictor when it is the only variable in the model ($ß_{con} = 0.048$, tstat = 3.43, $p = 0.01$).

3.3. Measures of contrast-dependent changes in LGN burst rate are not a trivial consequence of changes in firing rate

While the increase in burst rate with stimulus contrast is consistent with the biophysical properties of T-type Ca^{2+} channels, it is also possible that the increase in burst rate is not related to the involvement of T-type Ca^{2+} channels, but rather is a trivial consequence of the contrast-dependent changes in firing rate. As described above, when the contrast of a drifting grating is increased, there is increased excitation during the neuron's preferred phase and increased inhibition during the neuron's null phase. Consequently, there is an increase in the absolute number of high-frequency spikes (ISI <0.004s, Fig. 6A and C) and the number of long-ISI spikes (ISI >0.1s, Fig. 6B and C), as well as the probability of high-frequency spikes (Fig. 6D and F) and the probability of long ISI spikes (Fig. 6E and F). This raises the possibility that the increase in burst rate is a trivial consequence of the increased number of high-frequency spikes and long-ISI spikes. This explanation for the contrast-dependent increase in burst frequency assumes a Poisson distribution of LGN spike times; consequently, it can be accepted or ruled out by an analysis of the interdependence of high-frequency events and long-ISI spikes.

Under Poisson expectations, the probability of a high-frequency event, the second component of a burst, does not depend on the preceding ISI. However, consistent with the involvement of T-type Ca^{2+} channels, results show that the probability of a high-frequency spike is highly modulated by the preceding ISI for both low-contrast and high-contrast conditions (Fig. 7A–D). As predicted by the time/voltage relationship for de-inactivating T-Type Ca^{2+} channels (i.e., the greater the hyperpolarization, the less time required) the modulation of high-frequency probability was steeper and evident at shorter preceding ISIs with high-contrast stimuli compared with low-contrast stimuli. Importantly, this relationship was absent in the spike trains of retinal ganglion cells, which also experience increased preferred phase excitation and null-phase suppression, but do not exhibit bursting activity (Fig. 7E).

The modulation of high-frequency event probability by the preceding ISI clearly violates the assumption of Poisson distributions. However, it is possible that these non-Poisson spike interactions, including contrast-dependent increases in thalamic burst rate, can be accounted for by a time-varying Poisson spiking model that accounts for the sinusoidal nature of LGN firing rates in response to drifting sine-wave gratings. To examine this possibility, we simulated LGN spike rates using a time-varying Poisson model where the spike rates were set by a sinusoidal function and the neurons' firing rates (see Materials and Methods). In this way we quantified how the experimentally measured burst rates compared to burst rates seen in the simulated spike trains. If the contrast-dependent burst rate could be explained simply by the increase in firing rate, then we should observe similar burst rates in the experimental and simulated data.

Consistent with the involvement of T-type Ca^{2+} channels, the observed burst rate far exceeded the Poisson expectation during both low-contrast (Fig. 8A, experimental = 0.125±0.025, simulated = 0.009 ±0.0013, $p < 0.0015$, *t*-test) and high-contrast (Fig. 8B, experimental = 0.273±0.048, simulated = 0.0412±0.004, $p < 0.0015$, *t*-test) stimulation, indicating the involvement of nonlinear processes such as the voltage dependence of T-Type Ca^{2+} channels. Lastly, after removing the small, but present, "statistical" bursts (i.e., those occurring with Poisson expectation) from the observed measure of bursts, there remained a robust contrast-dependent increase in burst rate (Fig. 8C, low-contrast adjusted burst rate = 0.116 ±0.025, high-contrast adjusted burst rate = 0.232 ±0.048, $p = 0.009$, *t*-test).

4. Discussion

The goal of this study was to test the hypothesis that luminance contrast can influence the response mode (burst vs. tonic spiking) of LGN neurons. To explore the relationship between stimulus contrast and response mode, we recorded the activity of LGN neurons in the anesthetized cat during visual stimulation with low-contrast and high-contrast drifting sine-wave gratings. Fundamental to the reasoning behind these experiments was knowledge about the biophysical properties of the T-type Ca^{2+} channels that underlie bursts, assumptions about the membrane potential dynamics of LGN cells during stimulation with high- and low-contrast stimuli, and past work demonstrating bursts are unique events in the LGN and largely absent in the retina (Weyand, 2007; Alitto et al., 2019b; but see Sincich et al., 2007).

T-type channels have two gates, an inactivation gate and an activation gate (Tsien et al., 1988; Crunelli et al., 2005). For calcium entry to

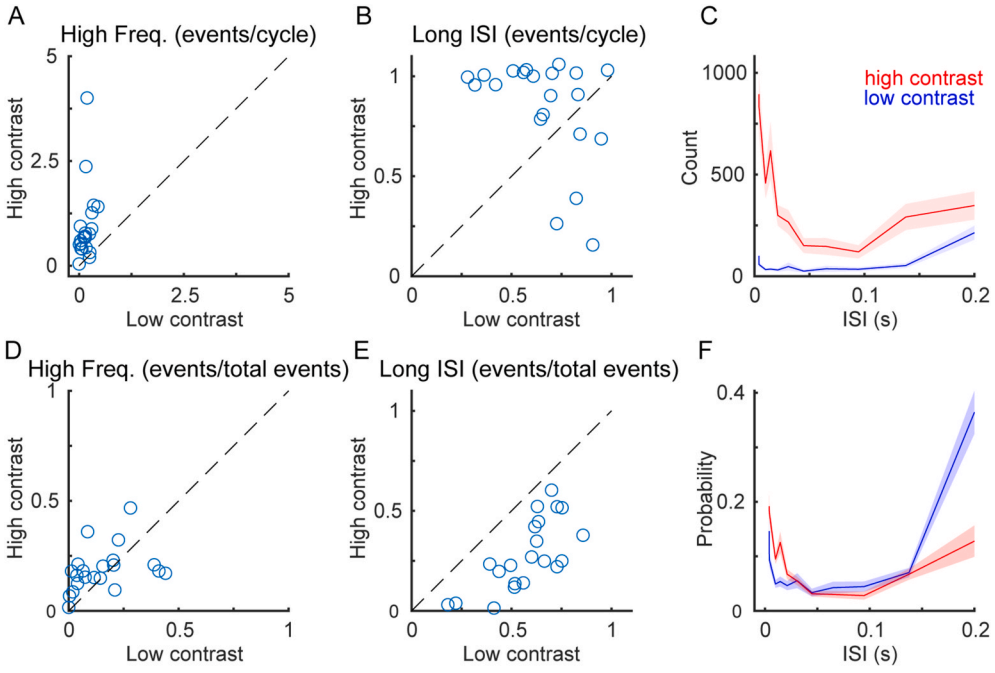

Fig. 6. Increasing stimulus contrast results in an increase in the total number of long-ISIs and high-frequency events. **A.** The number of high-frequency LGN events (ISI <4 ms, includes bursts) during low-contrast trials versus the number of high-frequency LGN events during high-contrast trials. **B.** The number of long-ISI LGN spikes (ISI >100 ms, includes bursts) during low-contrast trials versus the number of long-ISI LGN spikes during high-contrast trials **C.** Average distribution of LGN ISIs across the entire sample. **D-F.** Similar to A-C, but count has been converted to probability.

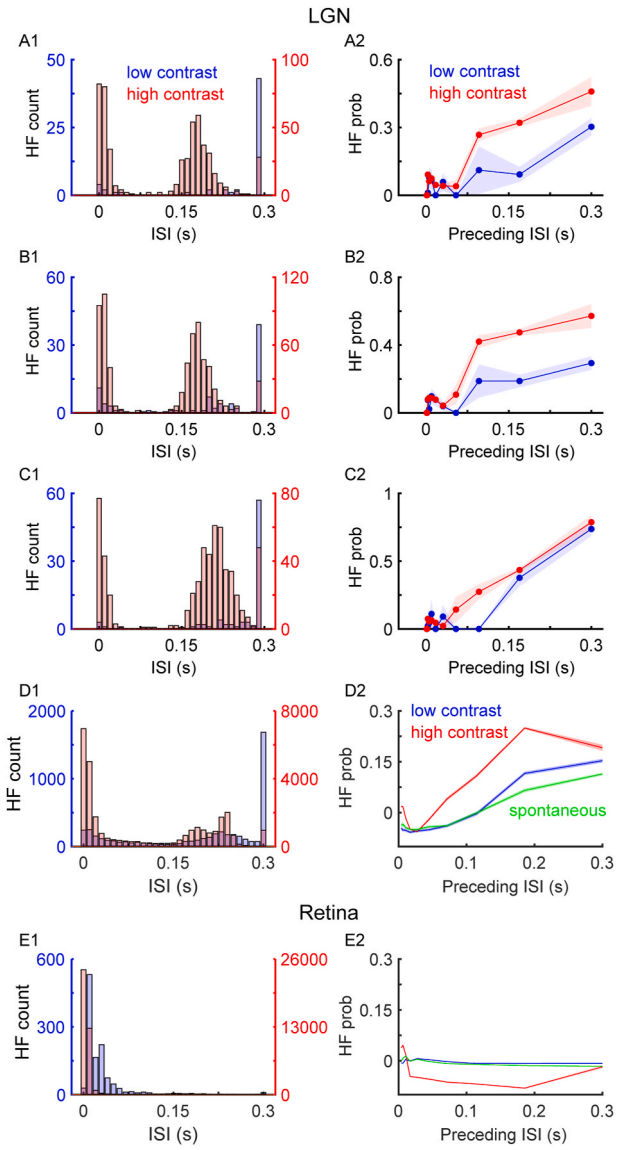

Fig. 7. The interdependence of long-ISIs and high-frequency events in the LGN. **A1.** Distribution of high-frequency events as a function of the preceding ISI for an example LGN neuron (blue = low-contrast trials, red = high-contrast trials). **A2.** The probability of high-frequency events as a function of preceding ISI. **B–C.** Similar to **A**, but for two additional, example LGN neurons. **D.** Similar to **A**, but for the entire sample of LGN neurons (green = spontaneous activity). **E.** Similar to **A**, but for the entire sample of retinal ganglion cells (green = spontaneous activity). (For interpretation of the references to colour in this figure legend, the reader is referred to the Web version of this article.)

occur, the inactivation gate must be in the de-inactivated state, a state that requires a sufficient period and depth of hyperpolarization (generally >100 ms and below a cell's typical resting potential), and the activation gate must be opened, a process that requires depolarization with voltage/time (δv/δt) constraints (Jahnsen and Llinás, 1984; Suzuki and Rogawski, 1989). Drifting gratings, with greater luminance modulation (higher contrast) and presumably greater membrane potential dynamics, would therefore seem better suited for opening T-type channels compared with gratings with less luminance modulation (lower contrast).

With opening of the T-type channels, Ca^{2+} influx evokes a T-potential that brings the membrane potential of a cell toward the threshold for activating voltage-gated Na^{+} channels (Jahnsen and Llinás, 1984; Suzuki and Rogawski, 1989). Because T-potentials last longer than the duration of an individual Na^{+} spike, a burst of Na^{+} spikes can ride on the T-potential (Wang et al., 1991; McCormick and Huguenard, 1992 Huguenard and McCormick, 1992; Huguenard, 1996; Perez-Reyes, 2003). However, if the T-type channels are inactivated and/or the δv/δt of depolarization is insufficient to open their activation gate, then depolarizing inputs to a cell will evoke tonic spikes without bursts, generally in proportion to the strength of their excitatory inputs. Consistent with these assumptions and predictions, we found the burst frequency, the number of spikes in a burst, and the timing precision of bursts were all significantly greater with higher contrast stimuli compared with lower contrast stimuli.

4.1. *Stimulus contrast affects the interspike interval (ISI) dynamics of bursts*

Based on results from intracellular recordings from which subthreshold T-potentials and suprathreshold bursts could be more clearly ascertained, two criteria were established for identifying burst events in extracellular recordings: (1) a preceding interspike interval (ISI) of >100 ms and (2) subsequent ISIs <4 ms (Fig. 1; Lu et al., 1992). The first criterion is believed to reflect the de-inactivation requirements of T-type Ca^{2+} channels; however, it is also known that the time/voltage relationship for de-inactivation is dynamic, with less time required for greater hyperpolarization and more time required for less hyperpolarization (McCormick and Huguenard, 1992; Huguenard and McCormick, 1992; Huguenard, 1996; Perez-Reyes, 2003). Consistent with this understanding, we found that high-frequency responses (ISIs < 4ms; the second criterion for a burst) were associated with shorter preceding ISIs (the first criterion for a burst) with higher contrast stimuli compared with lower contrast stimuli. This indicates that at higher contrast values (and presumably greater depth of hyperpolarization), the period of hyperpolarization (or ISI interval) needed to elicit a high-frequency burst is shortened from the generally accepted value of 100 ms. With lower contrast stimuli and in the absence of visual stimulation (i.e., spontaneous activity), the 100 ms criterion that is typically applied for identifying bursts was evident and seemed appropriate (Lu et al., 1992). These findings suggest that greater hyperpolarization not only increases the likelihood of a burst, but also shortens the time required to elicit a burst event.

4.2. *Contrast levels modulate the reliability of bursts*

An analysis of the timing of bursts with respect to the phase of the drifting grating revealed bursts occur more reliably and temporally precise with higher contrast stimuli compared with lower contrast stimuli. Moreover, at each contrast level (high or low) the timing of burst spikes was more consistent compared with the timing of tonic spikes. These findings likely also reflect the time-voltage relationship of T-type Ca^{2+}channels, with higher contrast stimuli having a greater δv/δt that results in a more reliable crossing of the T-channel threshold in a noisy background. Consistent with this view, results from a study using white-noise stimuli reported the suppressive phase of the spike-triggered average was significantly greater in magnitude and duration for burst spikes compared with tonic spikes (Alitto et al., 2005; see also Reinagel et al., 1999; Kepecs et al., 2002; Lesica and Stanley, 2004; Lesica et al., 2006; Zeldenrust et al., 2018; Mease et al., 2017). Similarly, previous work examining the temporal-frequency tuning properties of LGN neurons as a function of burstiness, reports LGN neurons shifting from low-pass to band-pass filtering with increased burstiness.

4.3. *Indirect inference of T-Type Ca^{2+} potentials*

Unlike studies using intracellular or whole-cell recording methods where the involvement of T-type Ca^{2+} channels in thalamic bursts can be directly assessed, studies using extracellular recording methods have relied on the criteria (preceding ISI >100 ms, subsequent ISIs <4 ms)

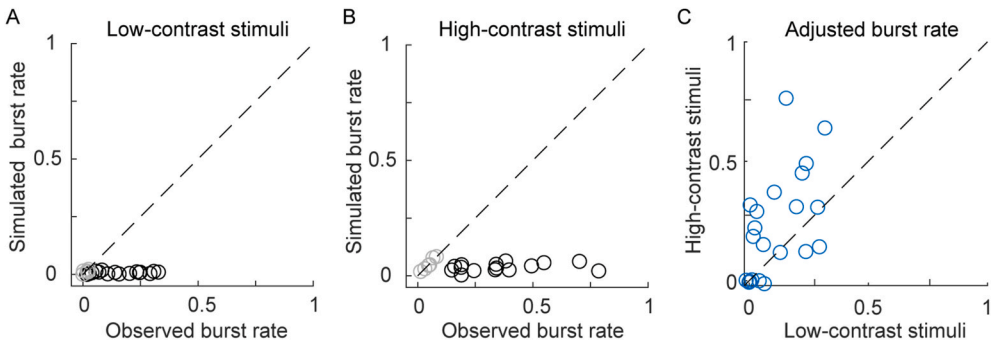

Fig. 8. Contrast-dependent changes in LGN bursting activity cannot be explained by changes in firing rate. **A.** Observed LGN burst rate as a function of the Poisson expectation during low-contrast visual stimulation ($p < 0.0015$, *t*-test; gray circles indicate no significant difference between observed and simulated burst rate, black circle indicate significant difference between observed and simulated burst rate). **B.** Similar to **A**, but for high-contrast stimulation ($p < 0.0015$, *t*-test). **C.** Scatterplot showing the adjusted burst rate (observed minus Poisson expectation) for LGN cells during high-contrast and low-contrast stimulation ($p = 0.009$, *t*-test).

established by Lu et al. (1992) to distinguish bursts. While these criteria have been shown to do an extremely good job at identifying bursts that rely on T-type Ca^{2+} channels, it must be acknowledged that misclassification can occur and that a single set of criteria may not apply equally well to different stimulus conditions and/or behavioral states. For instance, because the time required to de-inactivate (prime) T-type Ca^{2+} channels decreases as cells are more deeply hyperpolarized, it is likely that some thalamic bursts under these conditions with preceding ISIs <100 ms will be incorrectly excluded. Consistent with this view, there was an increase in high-frequency probability with high-contrast stimuli (and presumably greater null-phase hyperpolarization) with preceding ISIs <100 ms that was not seen with low-contrast stimuli (and presumably less null-phase hyperpolarization) (Fig. 7, panel D2; see also Alitto et al., 2019b).

Perhaps a larger concern is the occurrence of "statistical bursts", events identified as bursts that are simply the result of the temporal coincidence of a long preceding ISI followed by high-frequency spikes, without the involvement of T-type Ca^{2+} channels. This was a particular concern for the current study, as the possibility that the contrast-dependent increase in thalamic bursts might be a trivial consequence of the increase in firing rate (i.e., more statistical bursts at higher contrast). To address the possibility, we modeled LGN spiking using Poisson spiking statistics. A defining feature of Poisson processes is that each event occurs independent of every other event. Neuronal refractory periods, both absolute and relative, are a clear violation of Poisson assumptions; however, for the sake of simplicity, this biological inaccuracy was tolerated. A second violation of Poisson spiking relevant to this study is the phase-dependent, sinusoidal nature of LGN responses to drifting sine-wave gratings. This violation could not be ignored as it clearly affects the distribution of both long ISIs and high-frequency events. We therefore model LGN spiking as a sine function, with a firing rate set by the observed mean and f1, as the best approximation of LGN spiking that did not explicitly contain the non-Poisson characteristics associated with the biophysical properties of T-type Ca^{2+} channels. For most cells in this study (15/21), but not for cells with very low burst rates, results from this modeling effort indicate contrast-dependent bursting cannot be explained by the statistics of having higher firing rates. This finding, along with the small increase in the simulated burst rate under high-contrast conditions, emphasizes the importance of quantifying the possibility of statistical bursts in data collected in different conditions.

4.4. Bursts and thalamocortical processing

Our results show that LGN bursts can be driven by specific patterns of visual stimulation and that stimulus contrast affects burst frequency and timing. Similar findings have been reported for higher order thalamic neurons in the mouse whisker system (Mease et al., 2017), emphasizing the generality and importance of thalamic bursts across sensory systems. Moreover, all thalamic nuclei receive corticothalamic feedback from pyramidal neurons in layer 6 (reviewed in Usrey and Sherman, 2019). As this source of input can influence the membrane of thalamic neurons via monosynaptic excitation and disynaptic inhibition, layer 6 neurons have the opportunity to shift thalamic neurons between burst and tonic activity modes (Hirai et al., 2018; Mease et al., 2014). Provided there exists a cortical readout for bursts, bursts appear well suited for conveying contrast information to the cortex. Like other feedforward synapses, it is generally believed that thalamocortical synapses experience synaptic depression (Stratford et al., 1996; Gil et al., 1999; Chung et al., 2002). If so, then the long ISI that precedes a burst should reduce the amount of depression and thereby increase thalamocortical burst efficacy. In addition, the rapid train of spikes within a burst should evoke postsynaptic temporal summation (see Usrey et al., 2000; Usrey, 2002) and thereby lead to a similar increase in burst efficacy. Although direct measures of burst effectiveness in driving responses in visual cortex have yet to be performed, related studies have been performed in the somatosensory pathway of rabbits and mice where burst spikes are more effective than tonic spikes in driving cortical responses (Swadlow and Gusev, 2001) and increase the timing precision and spatial focus of cortical responses (Borden et al., 2022), respectively. If LGN bursts are similarly more effective at driving cortical responses, then visually evoked bursts would seem to have the properties needed to represent a distinct mode for processing and conveying visual information to the cortex.

CRediT authorship contribution statement

Alyssa N. Sanchez: contributed to the experimental design, data collection, Formal analysis, and writing of the manuscript. **Henry J. Alitto:** contributed to the experimental design, data collection, Formal analysis, and writing of the manuscript. **Daniel L. Rathbun:** contributed to the data collection and, Formal analysis. **Tucker G. Fisher:** contributed to the data collection and, Formal analysis. **W. Martin Usrey:** contributed to the experimental design, data collection, Formal analysis, and writing of the manuscript.

Declaration of competing interest

The authors declare the following financial interests/personal relationships which may be considered as potential competing interests: W. Martin Usrey reports financial support was provided by National Institutes of Health.

Data availability

Data will be made available on request.

Acknowledgements

We thank K.E. Neverkovec, D.J. Sperka, J.S. Johnson, and R. Oates

for expert technical assistance. This work was supported by NIH grants EY013588, EY015387, MH082174, and EY012576.

References

Alitto, H.J., Moore, B.D. 4th, Rathbun, D.L., Usrey, W.M., 2011. A comparison of visual responses in the lateral geniculate nucleus of alert and anaesthetized macaque monkeys. J. Physiol. 589, 87–99.

Alitto, H.J., Rathbun, D.L., Fisher, T.G., Alexander, P.C., Usrey, W.M., 2019a. Contrast gain control and retinogeniculate communication. Eur. J. Neurosci. 49, 1061–1068.

Alitto, H.J., Rathbun, D.L., Vandeleest, J.J., Alexander, P.C., Usrey, W.M., 2019b. The augmentation of retinogeniculate communication during thalamic burst mode. J. Neurosci. 39, 5697–5710.

Alitto, H.J., Weyand, T.G., Usrey, W.M., 2005. Distinct properties of stimulus-evoked bursts in the lateral geniculate nucleus. J. Neurosci. 25, 514–523.

Bereshpolova, Y., Stoelzel, C.R., Zhuang, J., Amitai, Y., Alonso, J.M., Swadlow, H.A., 2011. Getting drowsy? Alert/nonalert transitions and visual thalamocortical network dynamics. J. Neurosci. 31, 17480–17487.

Bezdudnaya, T., Cano, M., Bereshpolova, Y., Stoelzel, C.R., Alonso, J.M., Swadlow, H.A., 2006. Thalamic burst mode and inattention in the awake LGNd. Neuron 49, 421–432.

Borden, P.Y., Wright, N.C., Morrissette, A.E., Jaeger, D., Haider, B., Stanley, G.B., 2022. Thalamic bursting and the role of timing and synchrony in thalamocortical signaling in the awake mouse. Neuron 110, 2836–2853.

Butts, D.A., Cui, Y., Casti, A.R.R., 2016. Nonlinear computations shaping temporal processing of precortical vision. J. Neurophysiol. 116, 1344–1357.

Chung, S., Li, X., Nelson, S.B., 2002. Short-term depression at thalamocortical synapses contributes to rapid adaptation of cortical sensory responses in vivo. Neuron 34, 437–446.

Crunelli, V., Tóth, T.I., Cope, D.W., Blethyn, K., Hughes, S.W., 2005. The 'window' T-type calcium current in brain dynamics of different behavioural states. J. Physiol. 562, 121–129.

Dan, Y., Atick, J.J., Reid, R.C., 1996. Efficient coding of natural scenes in the lateral geniculate nucleus: experimental test of a computational theory. J. Neurosci. 16, 3351–3362.

Denning, K.S., Reinagel, P., 2005. Visual control of burst priming in the anesthetized lateral geniculate nucleus. J. Neurosci. 25, 3531–3538.

Deschenes, M., Paradis, M., Roy, J.P., Steriade, M., 1984. Electrophysiology of neurons of lateral thalamic nuclei in cat: resting properties and burst discharges. J. Neurophysiol. 51, 1196–1219.

Destexhe, A., Sejnowski, T.J., 2002. The initiation of bursts in thalamic neurons and the cortical control of thalamic sensitivity. Philos. Trans. R. Soc. Lond. B Biol. Sci. 357, 1649–1657.

Fisher, T.G., Alitto, H.A., Usrey, W.M., 2017. Retinal and non-retinal contributions to extraclassical surround suppression in the lateral geniculate nucleus. J. Neurosci. 37, 226–235.

Gil, Z., Connors, B.W., Amitai, Y., 1999. Efficacy of thalamocortical and intracortical synaptic connections: quanta, innervation, and reliability. Neuron 23, 385–397.

Guido, W., Lu, S.M., Vaughan, J.W., Godwin, D.W., Sherman, S.M., 1995. Receiver operating characteristic (ROC) analysis of neurons in the cat's lateral geniculate nucleus during tonic and burst response mode. Vis. Neurosci. 12, 723–741.

Hirai, D., Nakamura, K.C., Shibata, Ki, et al., 2018. Shaping somatosensory responses in awake rats: cortical modulation of thalamic neurons. Brain Struct. Funct. 223, 851–872.

Hong, S.Z., Kim, H.R., Fiorillo, C.D., 2014. T-type calcium channels promote predictive homeostasis of input-output relations in thalamocortical neurons of lateral geniculate nucleus. Front. Comput. Neurosci. 8, 98.

Hubel, D.H., Wiesel, T.N., 1961. Integrative action in the cat's lateral geniculate body. J. Physiol. 155, 385–398.

Huguenard, J.R., 1996. Low-threshold calcium currents in central nervous system neurons. Annu. Rev. Physiol. 58, 329–348.

Huguenard, J.R., McCormick, D.A., 1992. Simulation of the currents involved in rhythmic oscillations in thalamic relay neurons. J. Neurophysiol. 68, 1373–1383.

Jahnsen, H., Llinás, R., 1984. Electrophysiological properties of Guinea-pig thalamic neurones: an in vitro study. J. Physiol. 349, 205–226.

Kepecs, A., Wang, X.-J., Lisman, J., 2002. Bursting neurons signal input slope. J. Neurosci. 22, 9053–9062.

Kuffler, S.W., 1953. Discharge patterns and functional organization of mammalian retina. J. Neurophysiol. 16, 37–68.

Lesica, N.A., Stanley, G.B., 2004. Encoding of natural scene movies by tonic and burst spikes in the lateral geniculate nucleus. J. Neurosci. 24, 10731–10740.

Lesica, N.A., Weng, C., Jin, J., Yeh, C.-I., Alonso, J.-M., Stanley, G.B., 2006. Dynamic encoding of natural luminance sequences by LGN bursts. PLoS Biol. 4, e209.

Llinás, R., Jahnsen, H., 1982. Electrophysiology of mammalian thalamic neurones in vitro. Nature 297, 406–408.

Lu, S.M., Guido, W., Sherman, S.M., 1992. Effects of membrane voltage on receptive field properties of lateral geniculate neurons in the cat: contributions of the low-threshold Ca2+ conductance. J. Neurophysiol. 68, 1285–1298.

Martinez, L.M., Molano-Mazón, M., Wang, X., Sommer, F.T., Hirsch, J.A., 2014. Statistical wiring of thalamic receptive fields optimizes spatial sampling of the retinal image. Neuron 81, 943–956.

McCormick, D.A., Huguenard, J., 1992. A model of the electrophysiological properties of thalamocortical relay neurons. J. Neurophysiol. 68, 1384–1400.

Mease, R.A., Krieger, P., Groh, A., 2014. Cortical control of adaptation and sensory relay mode in the thalamus. Proc. Natl. Acad. Sci. USA 111, 6798–6803.

Mease, R.A., Kuner, T., Fairhall, A.L., Groh, A., 2017. Multiplexed spike coding and adaptation in the thalamus. Cell Rep. 19, 1130–1140.

Perez-Reyes, E., 2003. Molecular physiology of low-voltage-activated t-type calcium channels. Physiol. Rev. 83, 117–1161.

Rathbun, D.L., Alitto, H.J., Warland, D.K., Usrey, W.M., 2016. Stimulus contrast and retinogeniculate signal processing. Front. Neural Circ. 10, 8.

Rathbun, D.L., Warland, D.K., Usrey, W.M., 2010. Spike timing and information transmission at retinogeniculate synapses. J. Neurosci. 30, 13558–13566.

Reinagel, P., Godwin, D., Sherman, S.M., Koch, C., 1999. Encoding of visual information by LGN bursts. J. Neurophysiol. 81, 2558–2569.

Rivadulla, C., Martinez, L., Grieve, K.L., Cudeiro, J., 2003. Receptive field structure of burst and tonic firing in feline lateral geniculate nucleus. J. Physiol. 553, 601–610.

Sherman, S.M., Guillery, R.W., 2009. Exploring the Thalamus and its Role in Cortical Function, second ed. MIT Press, Cambridge, MA.

Sincich, L.C., Adams, D.L., Economides, J.R., Horton, J.C., 2007. Transmission of spike trains at the retinogeniculate synapse. J. Neurosci. 27, 2683–2692.

Stratford, K.J., Tarczy-Hornoch, K., Martin, K.A., Bannister, N.J., Jack, J.J., 1996. Excitatory synaptic inputs to spiny stellate cells in cat visual cortex. Nature 382, 258–261.

Sutter, E.E., 1987. A practical non-stochastic approach to nonlinear time-domain analysis. In: Advanced Methods of Physiological Systems Modeling, 1. University of Southern California, Los Angeles, pp. 303–315.

Suzuki, S., Rogawski, M.A., 1989. T-type calcium channels mediate the transition between tonic and phasic firing in thalamic neurons. Proc. Natl. Acad. Sci. USA 86, 7228–7232.

Swadlow, H.A., Gusev, A.G., 2001. The impact of 'bursting' thalamic impulses at a neocortical synapse. Nat. Neurosci. 4, 402–408.

Tsien, R.W., Lipscombe, D., Madison, D.V., Bley, K.R., Fox, A.P., 1988. Multiple types of neuronal calcium channels and their selective modulation. Trends Neurosci. 11, 431–438.

Usrey, W.M., 2002. Spike timing and visual processing in the retinogeniculocortical pathway. Phil. Trans. Roy. Soc. Lond.: Biol. Sci. 357, 1729–1737.

Usrey, W.M., Alitto, H.J., 2015. Visual functions of the thalamus. Annu. Rev. Vis. Sci. 1, 351–371.

Usrey, W.M., Alonso, J.M., Reid, R.C., 2000. Synaptic interactions between thalamic inputs to simple cells in cat visual cortex. J. Neurosci. 20, 5461–5467.

Usrey, W.M., Sherman, S.M., 2019. Corticofugal circuits: communication lines from the cortex to the rest of the brain. J. Comp. Neurol. 527, 640–650.

Usrey, W.M., Sherman, S.M., 2022. Exploring Thalamocortical Interactions: Circuitry for Sensation, Action, and Cognition. Oxford University Press.

Usrey, W.M., Reppas, J.B., Reid, R.C., 1998. Paired-spike interactions and synaptic efficacy of retinal inputs to the thalamus. Nature 395, 384–387.

Usrey, W.M., Reppas, J.B., Reid, R.C., 1999. Specificity and strength of retinogeniculate connections. J. Neurophysiol. 82, 3527–3540.

Vinck, M., van Wingerden, M., Womelsdorf, T., Fries, P., Pennartz, C.M.A., 2010. The pairwise phase consistency: a bias-free measure of rhythmic neuronal synchronization. Neuroimage 51, 112–122.

Wang, X.J., Rinzel, J., Rogawski, M.A., 1991. A model of the T-type calcium current and the low-threshold spike in thalamic neurons. J. Neurophysiol. 66, 839–850.

Wang, X., Wei, Y., Vaingankar, V., Wang, Q., Koepsell, K., Sommer, F.T., Hirsch, J.A., 2007. Feedforward excitation and inhibition evoke dual modes of firing in the cat's visual thalamus during naturalistic viewing. Neuron 55, 465–778.

Weyand, T.G., 2007. Retinogeniculate transmission in wakefulness. J. Neurophysiol. 98, 769–785.

Weyand, T.G., Boudreaux, M., Guido, W., 2001. Burst and tonic response modes in thalamic neurons during sleep and wakefulness. J. Neurophysiol. 85, 1107–1118.

Zeldenrust, F., Chameau, P., Wadman, W.J., 2018. Spike and burst coding in thalamocortical relay cells. PLoS Comput. Biol. 14, e1005960.